AMERICAN SOCIETY FOR MICROBIOLOGY | Molecular and Cellular Biology®

RESEARCH ARTICLE

Elucidation of the Role of FAM210B in Mitochondrial Metabolism and Erythropoiesis

Chie Suzuki,[a,b] Tohru Fujiwara,[a,b] Hiroki Shima,[c] Koya Ono,[a] Kei Saito,[a] Hiroki Kato,[a] Koichi Onodera,[a] Satoshi Ichikawa,[a] Noriko Fukuhara,[a] Yasushi Onishi,[a] Hisayuki Yokoyama,[a] Yukio Nakamura,[d] Kazuhiko Igarashi,[c] Hideo Harigae[a,b]

[a]Department of Hematology, Tohoku University Graduate School, Sendai, Japan
[b]Laboratory Diagnostics, Tohoku University Hospital, Sendai, Japan
[c]Department of Biochemistry, Tohoku University Graduate School of Medicine, Sendai, Japan
[d]Cell Engineering Division, RIKEN BioResourse Research Center, Tsukuba, Ibaraki, Japan

ABSTRACT Mitochondria play essential and specific roles during erythroid differentiation. Recently, *FAM210B*, encoding a mitochondrial inner membrane protein, has been identified as a novel target of GATA-1, as well as an erythropoietin-inducible gene. While FAM210B protein is involved in regulate mitochondrial metabolism and heme biosynthesis, its detailed function remains unknown. Here, we generated both knockout and knockdown of endogenous FAM210B in human induced pluripotent stem-derived erythroid progenitor (HiDEP) cells using CRISPR/Cas9 methodology. Intriguingly, erythroid differentiation was more pronounced in the FAM210B-depleted cells, and this resulted in increased frequency of orthochromatic erythroblasts and decreased frequencies of basophilic/polychromatic erythroblasts. Comprehensive metabolite analysis and functional analysis indicated that oxygen consumption rates and the NAD (NAD^+)/NADH ratio were significantly decreased, while lactate production was significantly increased in FAM210B deletion HiDEP cells, indicating involvement of FAM210B in mitochondrial energy metabolism in erythroblasts. Finally, we purified FAM210B-interacting protein from K562 cells that stably expressed His/biotin-tagged FAM210B. Mass spectrometry analysis of the His/biotin-purified material indicated interactions with multiple subunits of mitochondrial ATP synthases, such as subunit alpha (ATP5A) and beta (ATP5B). Our results suggested that FAM210B contributes prominently to erythroid differentiation by regulating mitochondrial energy metabolism. Our results provide insights into the pathophysiology of dysregulated hematopoiesis.

KEYWORDS FAM210B, mitochondria, erythroid differentiation, mitochondrial ATP synthase

GATA-1 is the founding member of the GATA family of transcription factors. This family contains a zinc finger domain that recognizes the DNA-binding consensus site (A/T)GATA(A/G) (1) in gene promoters. GATA-1 is critical for erythroid differentiation, as shown by cell-based *ex vivo* assays and gene deletion mouse models (2–4). GATA-1 regulates the expression of numerous erythroid-specific genes, including erythroid transcription factors, signaling molecules, and membrane proteins (5–7). Despite much research on the GATA-1 family, there are many uncharacterized genes that may contribute to erythroid differentiation *in vivo* (5–7). Given the pleiotropic roles of GATA-1-regulated genes, it is likely that identification and characterization of novel GATA-1 target genes would provide valuable new insights into erythroid biology (4, 5).

Mitochondria play essential and specific roles during erythroid differentiation. In early-lineage commitment from hematopoietic stem cells, mitochondria regulate the progression from pluripotency to a differentiated state (8). In late erythropoiesis, mitochondria play a role in iron metabolism and heme biosynthesis and in reticulocyte maturation (8, 9).

Address correspondence to Tohru Fujiwara, fujiwara-to@med.tohoku.ac.jp.

The authors declare no conflict of interest.

Received 13 April 2022
Returned for modification 15 May 2022
Accepted 20 October 2022
Published 14 November 2022

Mitochondria drive their own elimination through mitophagy in the process of erythrocyte maturation (10, 11). The transition from cell expansion to cell differentiation has been correlated with a metabolic switch from glycolysis to oxidative phosphorylation; however, these activities during erythroid differentiation remain to be fully elucidated. We recently identified the gene encoding the mitochondrial protein; that is *FAM210B* (indicating the family with sequence similarity 210 member B, also known as *C20orf108*) as a previously unrecognized target of GATA-1 (12). The *FAM210B* gene encodes an inner mitochondrial protein and is abundantly expressed in the later stages of erythroid differentiation (12, 13). While studies in breast cancer cells have suggested that the FAM210B protein may regulate mitochondrial oxidation (14), its detailed function in primary erythroblasts remains is unknown.

In the present study, we extended the characterization of FAM210B protein in erythroid cells. We generated FAM210B-deficient cells using CRISPR/Cas9-based genome editing and conducted comprehensive metabolite analysis to reveal the role of FAM210B in mitochondrial metabolism during erythroid differentiation. We performed mass spectrometry to identify proteins that coimmunoprecipitated with His/biotin-tagged FAM210B and reveal detailed mechanistic insights.

RESULTS

Generation of *FAM210B*-depleted erythroid progenitor cell lines. First, we conformed that endogenous FAM210B protein was abundantly detected in a mitochondrial fraction of HiDEP cells (Fig. 1A). Then, we generated both *FAM210B*-knockdown and -knockout HiDEP cell lines (Fig. 1B to D) with CRISPR/Cas9-mediated gene editing to rule out the possibility of an off-target effect. No significant impact on cell proliferative activity was observed with *FAM210B* depletion in HiDEP cells (Fig. 1E). There was also no significant impact on either the intracellular heme concentration (Fig. 1F) or the expression of erythroid-related genes, such as *ALAS2* (5′-aminolevulinate synthase 2), *HBG* (hemoglobin subunit gamma), *HBA* (hemoglobin subunit alpha), and *HMOX1* (heme oxygenase 1; Fig. 1G). We compared gene expression profiling in FAM210B-knockout and control HiDEP cells to predict the consequences of FAM210B depletion. The analysis revealed >1.5-fold up- and downregulation of 100 and 56 genes, respectively (Fig. 1H; see also Table S1 in the supplemental material). Quantitative RT-PCR-based validation analysis confirmed upregulation of the genes asparagine synthase (*ASNS*) and aldo-keto reductase family 1 member B (*AKR1B1*) and downregulation of the gene tetratricopeptide repeat domain 19 (*TTC19*) in FAM210B-knockout HiDEP cells (Fig. 1I). GO analysis identified significant enrichment of genes involved in extracellular vesicle and RNA binding ($P = 0.01$ and 0.04, respectively; Fig. 1J). Of note, the downregulated cohort includes *TTC19*, which encodes a protein involved in mitochondrial respiratory chain complex III assembly (15); mitochondrial alanyl-tRNA synthase (*AARS2*), which can contribute to mitochondrial cardiomyopathy (16); and chloride intracellular channel 1 (*CLIC1*), which regulates mitochondrial membrane potential (17) (Fig. 1H; see also Table S1). On the other hand, the upregulated cohort includes mitochondrial ribosomal protein L53 (*MRPL53*), transmembrane protein 126A (*TMEM126A*), which is located at mitochondrial inner membrane and is necessary for the correct function of mitochondrial complex I (18), cytochrome c_1 (*CYC1*), which is a heme-containing subunit of mitochondrial complex III and is required for energy production (19), NADH:ubiquinone oxidoreductase subunit B1 (*NDUFB1*), which is a component of mitochondrial complex I (20), pyruvate dehydrogenase complex component X (*PDHX*), which is located at mitochondrial matrix and is involved in the pathophysiology of Leigh's disease (21), and pantothenate kinase 2 (*PANK2*), which encodes an enzyme critical for the biosynthesis of coenzyme A (22) (Fig. 1H; see also Table S1 in the supplemental material). Thus, while the GO analysis failed to identify significant enrichment of genes involved in mitochondrial biology, FAM210B depletion in erythroblasts might be associated with altered mitochondrial metabolism.

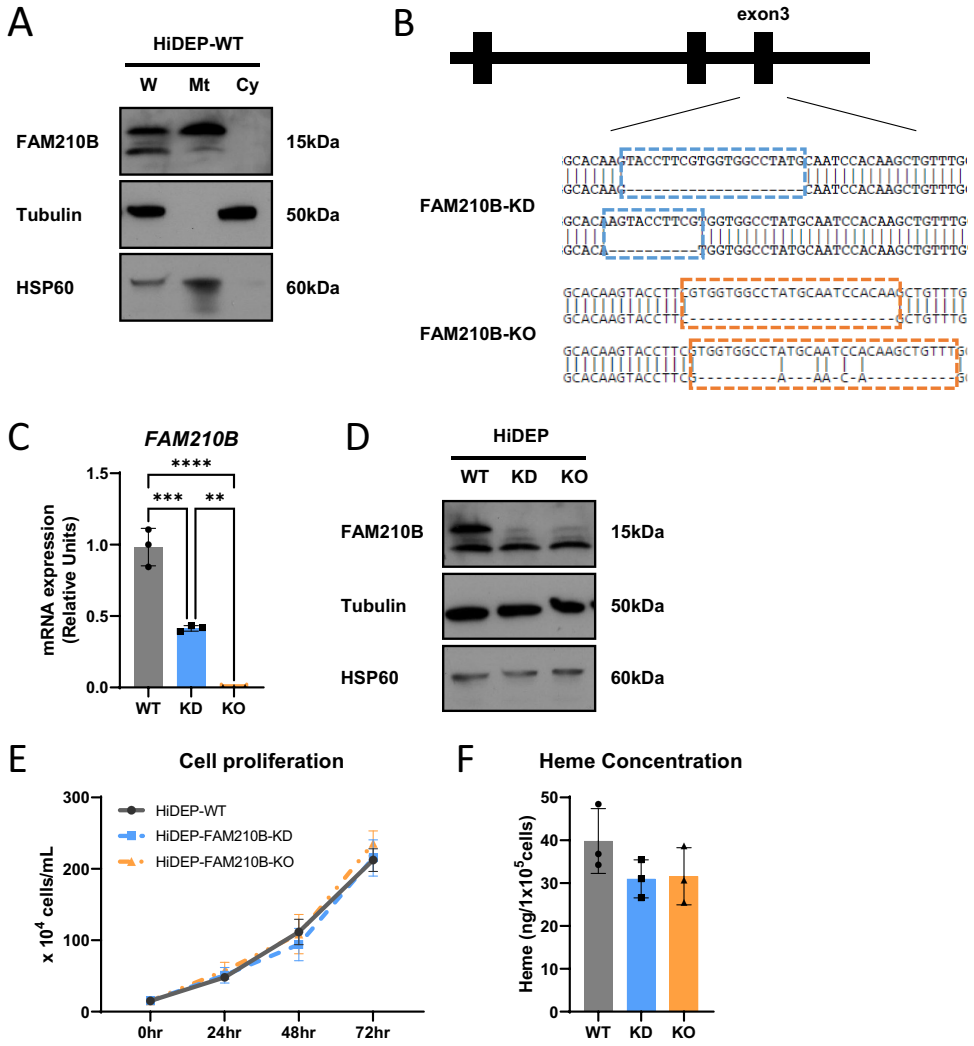

FIG 1 Deletion of endogenous *FAM210B* in HiDEP cells. (A) Western blot analysis to detect endogenous FAM210B protein in HiDEP cells. Whole-cell lysates (W) were separated into mitochondrial (Mt) and cytosolic (Cy) fractions, with the purity of each fraction validated based on α-tubulin (cytosolic) and HSP60 (mitochondrial). (B) Sequence analysis of FAM210B-KD (knockdown) and FAM210B-KO (knockout) HiDEP cells. (C and D) Quantitative RT-PCR analysis (C) and Western blot analysis (D) of FAM210B and HSP60 expression in wild-type, FAM210B-KD (knockdown), and FAM210B-KO (knockout) HiDEP cells (n = 3, means $\pm$ the standard deviations [SD]). Each mRNA level was normalized to *GAPDH* (*, $P < 0.05$; **, $P < 0.01$; ***, $P < 0.001$; ****, $P < 0.0001$). Blots probed with anti-α-tubulin were used as loading controls. (E and F) Changes in the total numbers of cells (E) and intracellular heme concentrations (F) by FAM210B knockdown or knockout (n = 3, means $\pm$ the SD). (G) Quantitative RT-PCR analysis of transcripts encoding ALAS2, HBG, HBA, and HMOX1 in wild-type, *FAM210B*-KD, and *FAM210B*-KO HiDEP cells, all normalized to GAPDH (n = 3, means $\pm$ the SD; *, $P < 0.05$; **, $P < 0.01$). (H) Expression profiling of wild-type and FAM210B-KO HiDEP cells. The heat map depicts the fold changes in expression secondary to *FAM210B* knockout; the 50 most upregulated and most downregulated genes are shown. (I) Quantitative RT-PCR analysis of transcripts encoding ASNS, AKR1B1, and TTC19 in wild-type, *FAM210B*-KD, and *FAM210B*-KO HiDEP cells, all normalized to GAPDH (n = 3, means $\pm$ the SD; *, $P < 0.05$; **, $P < 0.01$). (J) Gene Ontology (GO) analysis for differentially expressed genes by >1.5-fold after FAM210B knockout.

Erythroid differentiation was more pronounced in *FAM210B*-depleted HiDEP cells. Studies on human and mouse primary erythroblasts indicated that *FAM210B* undergoes upregulation during later stages of erythroid differentiation (12, 13). HiDEP cells largely correspond to the proerythroblast stage (23) and, as such, phenotypic changes resulting from FAM210B depletion might be difficult to detect (Fig. 1). Thus, we differentiated *FAM210B*-depleted HiDEP clones from later-stage erythroblasts by coculturing with OP9 stromal cells and the addition of ferrous iron (24) (Fig. 2A). We first evaluated *FAM210B* mRNA expression kinetics for up to 10 days during erythroid

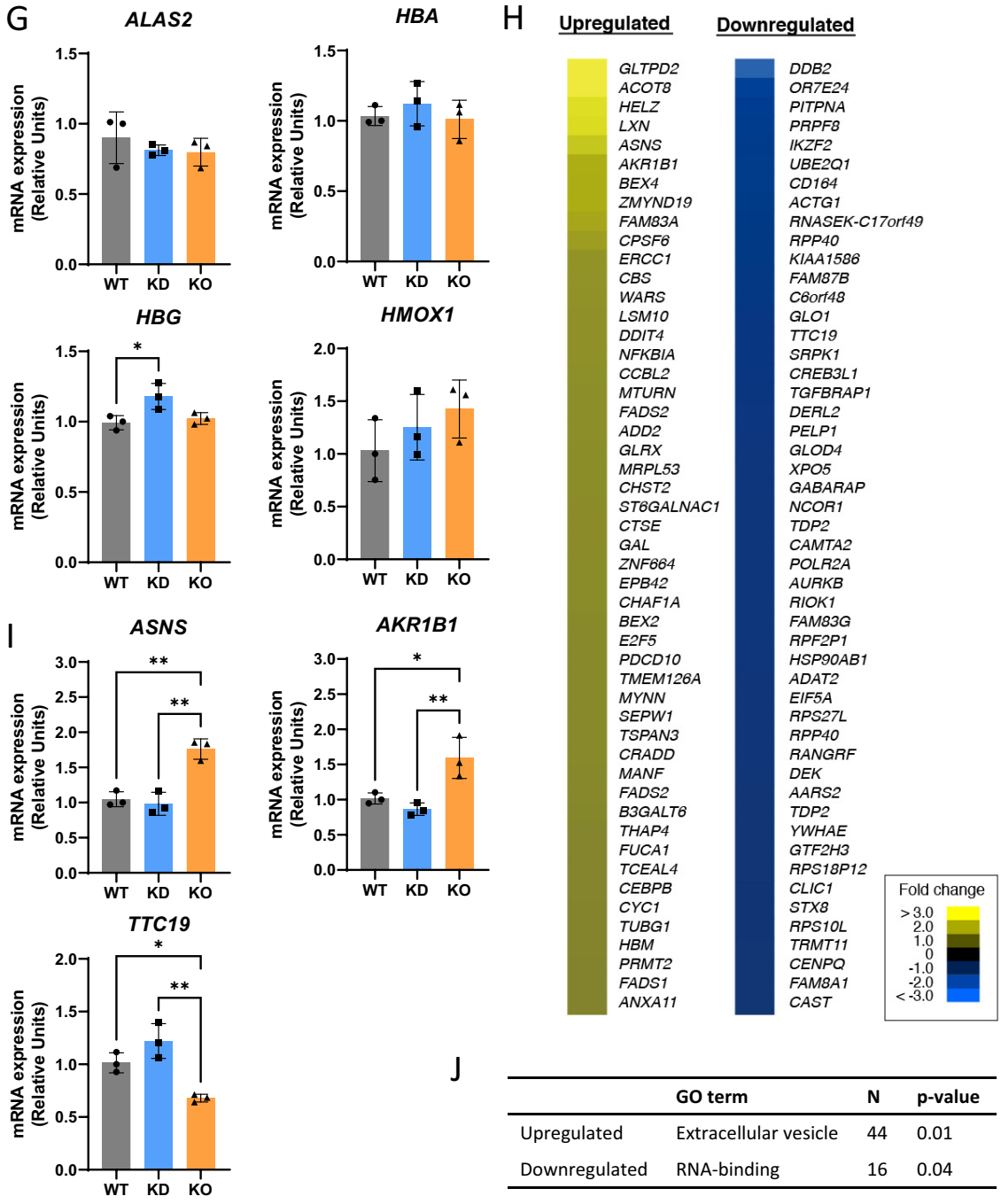

J

	GO term	N	p-value
Upregulated	Extracellular vesicle	44	0.01
Downregulated	RNA-binding	16	0.04

FIG 1 (Continued)

differentiation of wild-type HiDEP cells. We then confirmed that expression was upregulated in the later stages of erythroid differentiation (Fig. 2B and C). The *FAM210B* expression pattern was similar to the pattern observed with other GATA-1 target genes (*ALAS2*, *HBA*, and *HBB*) as well as *HMOX1*, which was also upregulated in the later stage of erythroid differentiation (25). In addition, the oxygen consumption rate (OCR) was significantly decreased with induction of erythroid differentiation (Fig. 2D), indicating that erythroid differentiation was accompanied by decreased mitochondrial activity. To estimate the consequences of decreased OCR on mitochondrial metabolism, we evaluated the expression of *SLC16A1*, encoding lactate transporter MCT1 (26), demonstrating that the gene was moderately increased in a later stage of erythroid differentiation

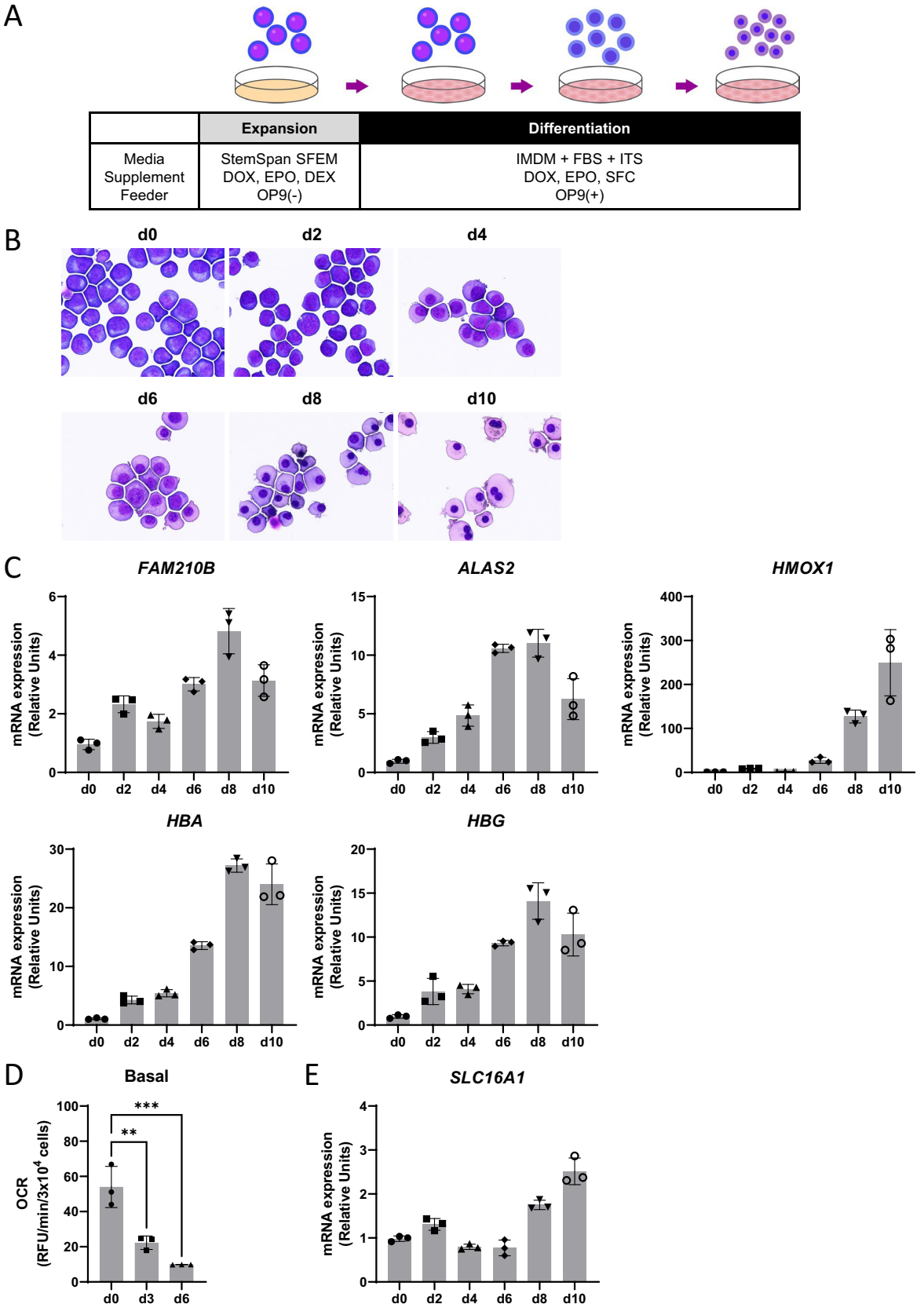

FIG 2 Kinetics of FAM210B expression during erythroid differentiation of HiDEP cells. (A) Protocol for erythroid differentiation of HiDEP cells. SFC, sodium ferrous citrate; IMDM, Iscove modified Dulbecco medium. (B) May-Grunewald-Giemsa staining of wild-type HiDEP cells in

(Continued on next page)

(Fig. 2E). Though we did not directly evaluate lactate levels, the results might imply that lactate levels were increased during erythroid differentiation.

Intriguingly, we found that *FAM210B*-knockdown and -knockout cells exhibited a higher proportion of orthochromatic erythroblasts and a lower proportion of basophilic/polychromatic erythroblasts at day 6 of differentiation (Fig. 3A and B). This indicated promotion of erythroid differentiation. Concomitantly, the intracellular heme concentration at day 6 was significantly enhanced by FAM210B depletion (Fig. 3C). Flow cytometric analysis suggested that erythroid differentiation was more pronounced in FAM210B-depleted HiDEP cells upon inducing erythroid differentiation on day 4, as indicated by marginally increased frequency of $CD235a^+/CD71^-$ in FAM210B-knockout cells (Fig. 3D). Quantitative RT-PCR analysis confirmed significant upregulation of erythroid genes (i.e., *ALAS2*, *HBG*, *HBA*, and *HMOX1*), as well as *SLC2A1*, which encodes glucose transporter (GLUT1), which is abundantly expressed in erythrocytes (27) (Fig. 3E). Taken together, these findings show that HiDEP cells are capable of more profound erythroid differentiation after the depletion of endogenous FAM210B.

FAM210B is involved in mitochondrial energy metabolism. Based on the potential role of FAM210B in mitochondrial energy metabolism (Fig. 1), we evaluated OCR in both wild-type and FAM210B-depleted cells. As shown in Fig. 4A, *FAM210B*-depleted HiDEP cells exhibited significantly lower OCR. Although oxidative phosphorylation is tightly associated with ATP production, the ATP level in the culture medium was not significantly decreased by FAM210B depletion (Fig. 4B). While glucose consumption was not affected, lactate production in the culture medium was significantly increased with FAM210B knockout (Fig. 4C and D), indicating a shift toward anaerobic glycolysis. Because lactic acidosis could be induced by dysfunction of the mitochondrial complex I (28), which is responsible for controlling the NAD^+/NADH redox ratio, we also evaluated the status of NAD^+/NADH (Fig. 4E), demonstrating that the ratio was significantly decreased by FAM210B depletion. Because accumulation of lactate could be induced by the dysfunction of mitochondrial pyruvate carrier (MPC1 and MPC2) (29, 30), we evaluated the expressions of these genes, demonstrating that FAM210B depletion did not significantly compromise the expression of MPCs (Fig. 4F and G).

Next, we elucidated the global metabolic changes induced by FAM210B depletion. We confirmed weakly decreased intracellular ATP levels in FAM210B depleted cells (relative areas, 0.0321 and 0.0225 for wild-type cells and FAM210B knockout HiDEP cells, respectively; Fig. 5A; see also Table S2). In contrast to increased lactate level in the culture media (Fig. 4D), intracellular lactate levels were not significantly increased by FAM210B knockout (Fig. 4H and 5A). In addition, the analysis indicated that metabolites derived from acetyl coenzyme A (acetyl-CoA), such as citric acid and isocitric acid, were decreased by FAM210B depletion, whereas the α-ketoglutaric acid (2-oxoglutaric acid [2-OG]) level was almost comparable, indicating that tricarboxylic acid (TCA) cycle activity might not be globally compromised by FAM210B depletion (Fig. 5A and B; see also Table S2). Based on electron microscopy assessment, we noticed smaller mitochondrial sizes with FAB210B depletion (Fig. 5C), while the total amount of mitochondria was not significantly affected (Fig. 5D). We also quantified the amount of mitochondrion-specific protein (HSP60), as well as mtDNA (Fig. 1D and 5F), demonstrating that FAM210B depletion did not affect mitochondrial content. Taken together, these results indicated that FAM210B may be involved in mitochondrial energy metabolism in erythroblasts.

FAM210B interacts with multiple subunits of mitochondrial ATP synthases. Human FAM210B is a mitochondrial inner membrane protein that has been predicted to function as an adaptor protein (12, 13). We hypothesized that FAM210B may interact

FIG 2 Legend (Continued)
coculture with OP9 stromal cells for 0, 2, 4, 6, 8, and 10 days. (C) Quantitative RT-PCR analysis of transcripts encoding FAM210B, ALAS2, HMOX1, HBG, and HBA during erythroid differentiation of wild-type HiDEP cells for 0, 2, 4, 6, 8, and 10 days, normalized to GAPDH (n = 3, means ± the SD). (D) Basal oxygen consumption rate (OCR) in wild-type HiDEP cells at days 0, 3, and 6 of erythroid differentiation (n = 3, means ± the SD; *, $P < 0.05$). (E) Quantitative RT-PCR analysis of transcripts encoding SLC16A1 during erythroid differentiation of wild-type HiDEP cells for 0, 2, 4, 6, 8, and 10 days, normalized to GAPDH (n = 3, means ± the SD).

A

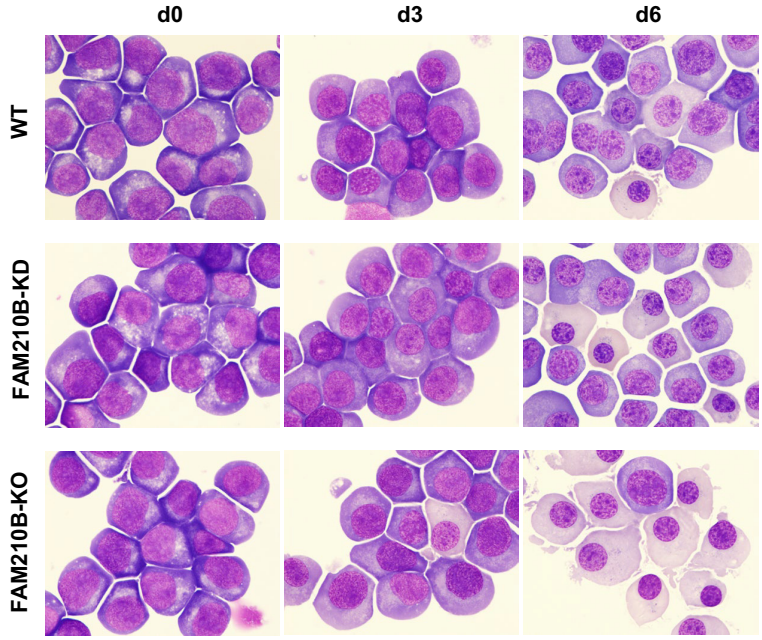

B

	WT	FAM210B-KD	FAM210B-KO
Proerythroblast	2.5 ± 2.2	2.8 ± 1.6	1.8 ± 1.3
Basophilic erythroblast	14.2 ± 2.0	11.8 ± 1.0	7.0 ± 3.0*
Polychromatic erythroblast	75.7 ± 0.3	64.0 ± 1.3***	55.5 ± 2.0****
Orthochromatic erythroblast	7.7 ± 0.3	21.3 ± 1.5***	35.7 ± 3.5****

C

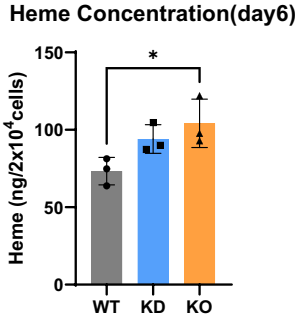

FIG 3 Promotion of erythroid differentiation by FAM210B depletion in HiDEP cells. (A) May-Grunewald-Giemsa staining of wild-type, *FAM210B*-KD, and *FAM210B*-KO HiDEP cells in coculture with OP9 stromal cells for 0, 3, and 6 days. (B) Frequency of proerythroblasts (Pro), basophilic erythroblasts (Baso), polychromatic erythroblasts (Poly), and orthochromatic erythroblasts (Ortho) generated from wild-type (WT), *FAM210B*-KD, and *FAM210B*-KO HiDEP cells cocultured with OP9 stromal cells in with SFC for 6 days (*, $P < 0.05$; **, $P < 0.01$; ***, $P < 0.001$; ****, $P < 0.0001$ [compared to WT]). (C) Heme concentrations in wild-type, *FAM210B*-KD, and *FAM210B*-KO HiDEP cells in coculture with OP9 stromal cells for 6 days (*, $P < 0.05$). (D) (Left) FACS analysis based on wild-type, *FAM210B*-KD, and *FAM210B*-KO HiDEP cells in coculture with OP9 stromal cells for 4 days. The result is representative of three independent experiments. (Right) Summary of the frequency of $CD235a^+/CD71^-$ cells on days 0 and 4 of differentiation ($n = 3$, means ± the SD). (E) Quantitative RT-PCR analysis of *FAM210B*, *ALAS2*, *HBG*, *HBA*, *HMOX1*, and *SLC2A1* mRNA, all normalized to GAPDH in wild-type, *FAM210B*-KD, and *FAM210B*-KO HiDEP cells in coculture with OP9 stromal cells for 0, 3, and 6 days ($n = 3$, means ± the SD; *, $P < 0.05$; **, $P < 0.01$; ***, $P < 0.001$; ****, $P < 0.0001$.).

directly with many mitochondrial proteins and may be involved in mitochondrial energy metabolism. To explore this issue, FAM210B-interacting proteins were purified from genetically modified K562 cells that stably expressed His/biotin-tagged FAM210B (Fig. 6A and B). Our results showed significant enrichment of multiple subunits of mitochondrial ATP synthases in association with FAM210B, especially subunits alpha

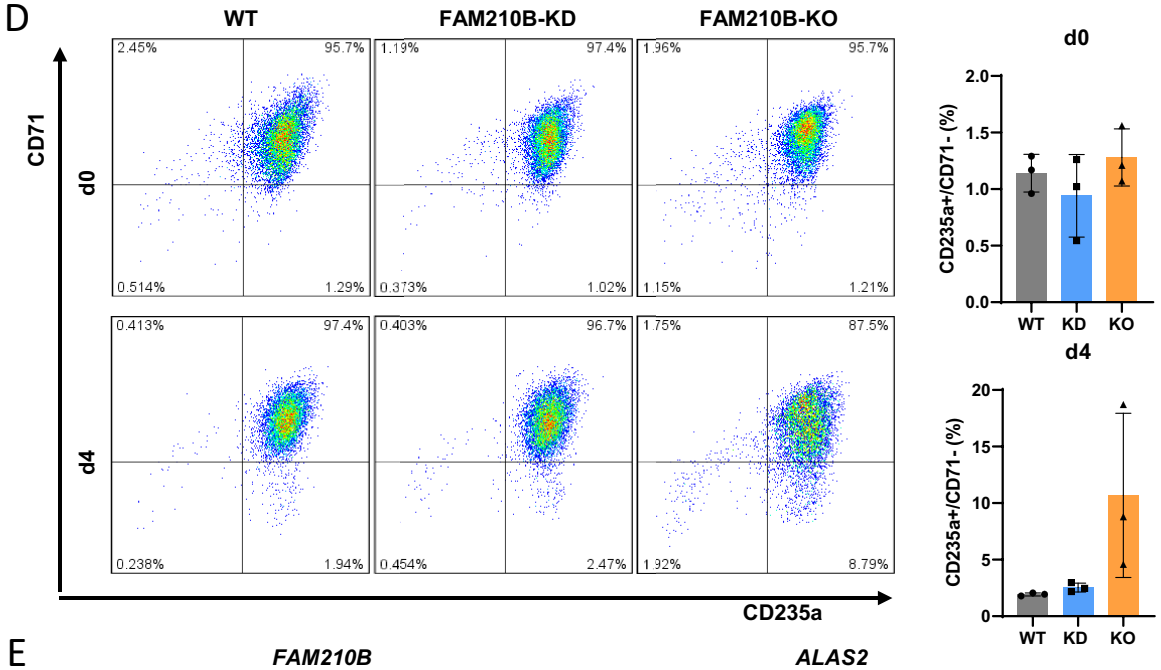

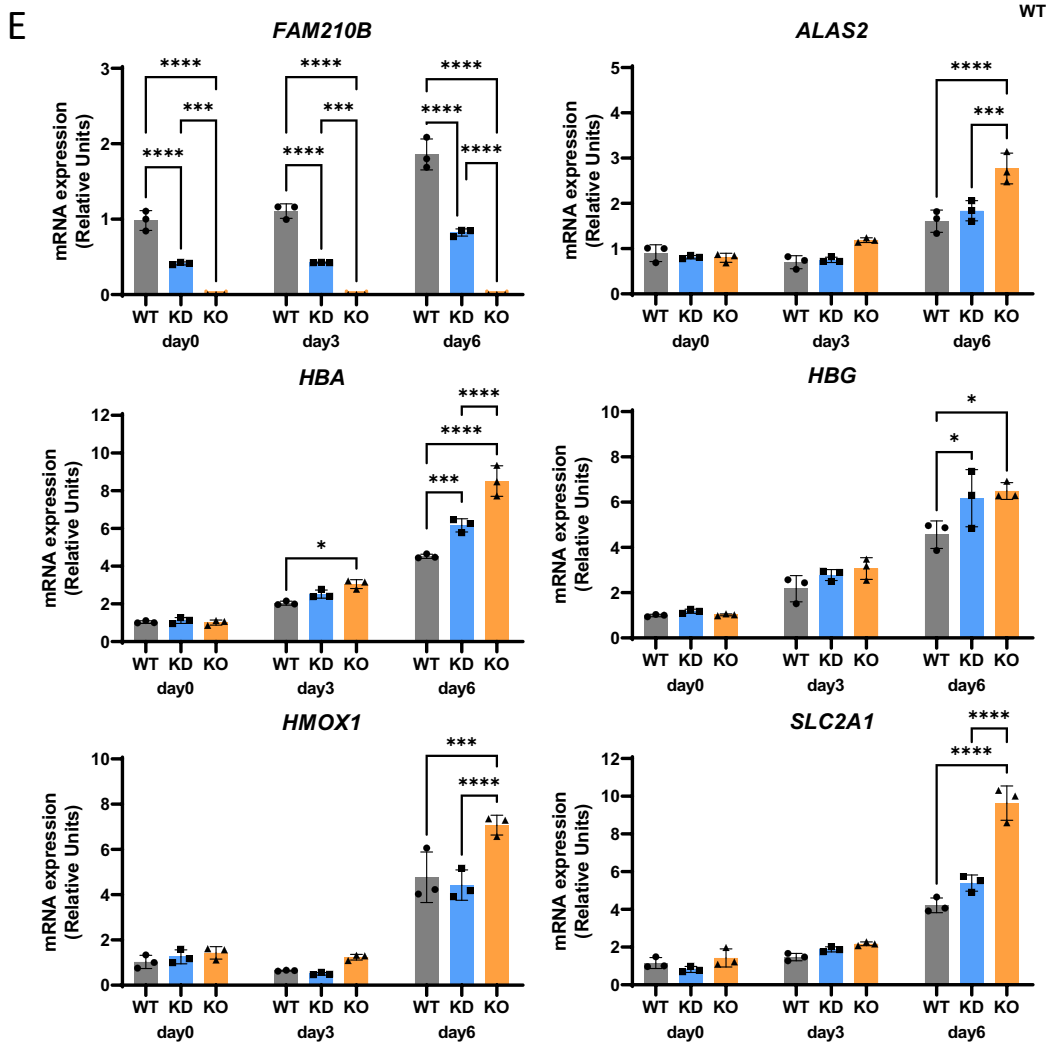

FIG 3 (Continued)

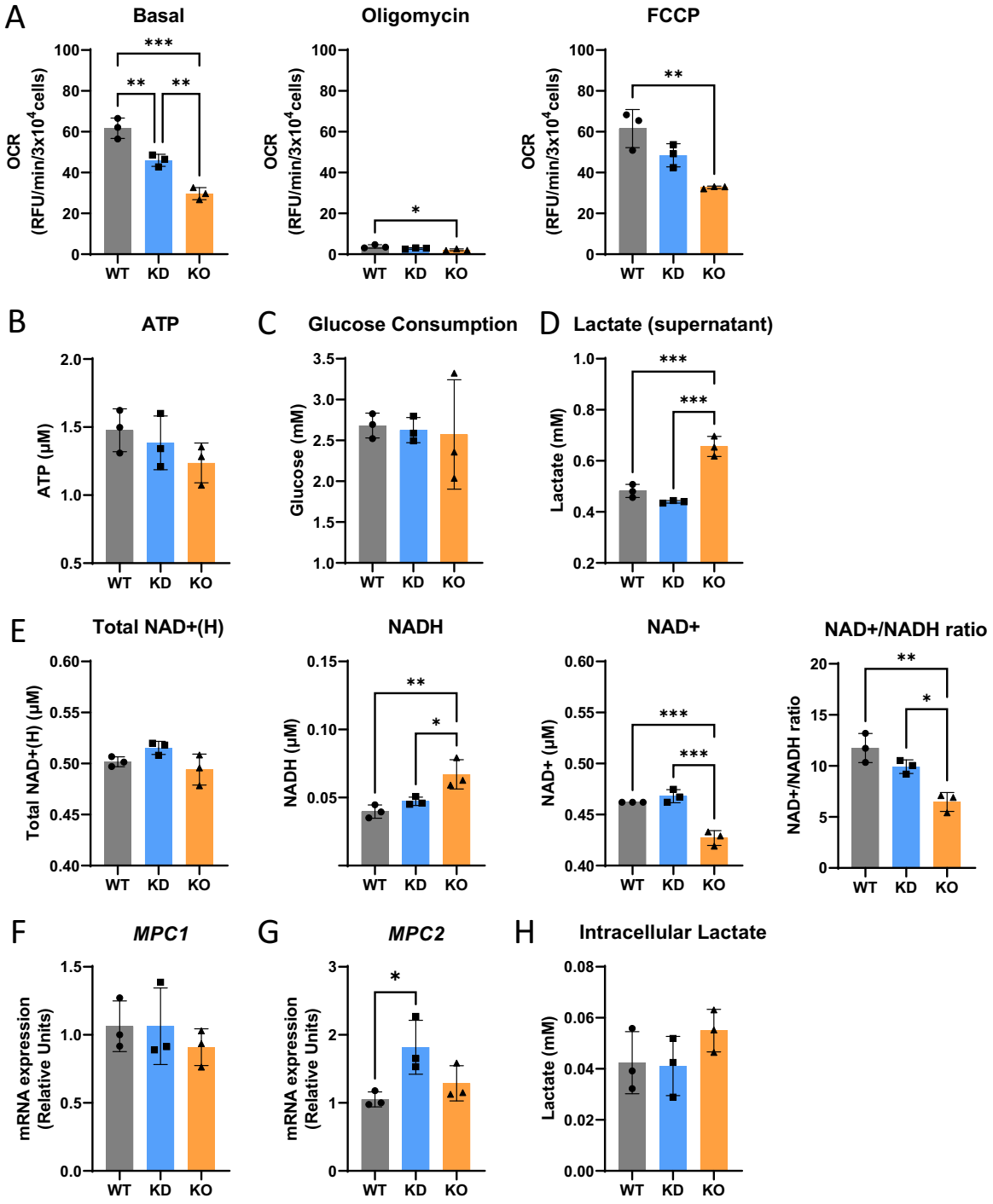

FIG 4 Altered mitochondrial metabolism by FAM210B depletion. (A) Basal and maximum (FCCP-treated) oxygen consumption rates in wild-type, *FAM210B*-KD, and *FAM210B*-KO HiDEP cells shown at day 3 of erythroid differentiation ($n = 3$, means ± the SD; *, $P < 0.05$; **, $P < 0.01$; ***, $P < 0.001$). (B to D) ATP production (B), glucose consumption (C), and lactate production in the culture supernatant (D) in wild-type, FAM210B-KD, and FAM210B-KO HiDEP cells ($n = 3$, means ± the SD; *, $P < 0.05$; **, $P < 0.01$; ***, $P < 0.001$). (E) Total NAD^+(H) level, NADH level, NAD^+ level, and NAD^+/NADH ratio (right) in wild-type, FAM210B-KD, and FAM210B-KO HiDEP cells ($n = 3$, means ± the SD; *, $P < 0.05$). (F and G) Quantitative RT-PCR analysis of *MPC1* (F) and *MPC2* (G) mRNA, all normalized to GAPDH in wild-type, *FAM210B*-KD, and *FAM210B*-KO HiDEP cells ($n = 3$, means ± the SD; *, $P < 0.05$). (H) Intracellular lactate level in wild-type, *FAM210B*-KD, and *FAM210B*-KO HiDEP cells ($n = 3$, means ± the SD).

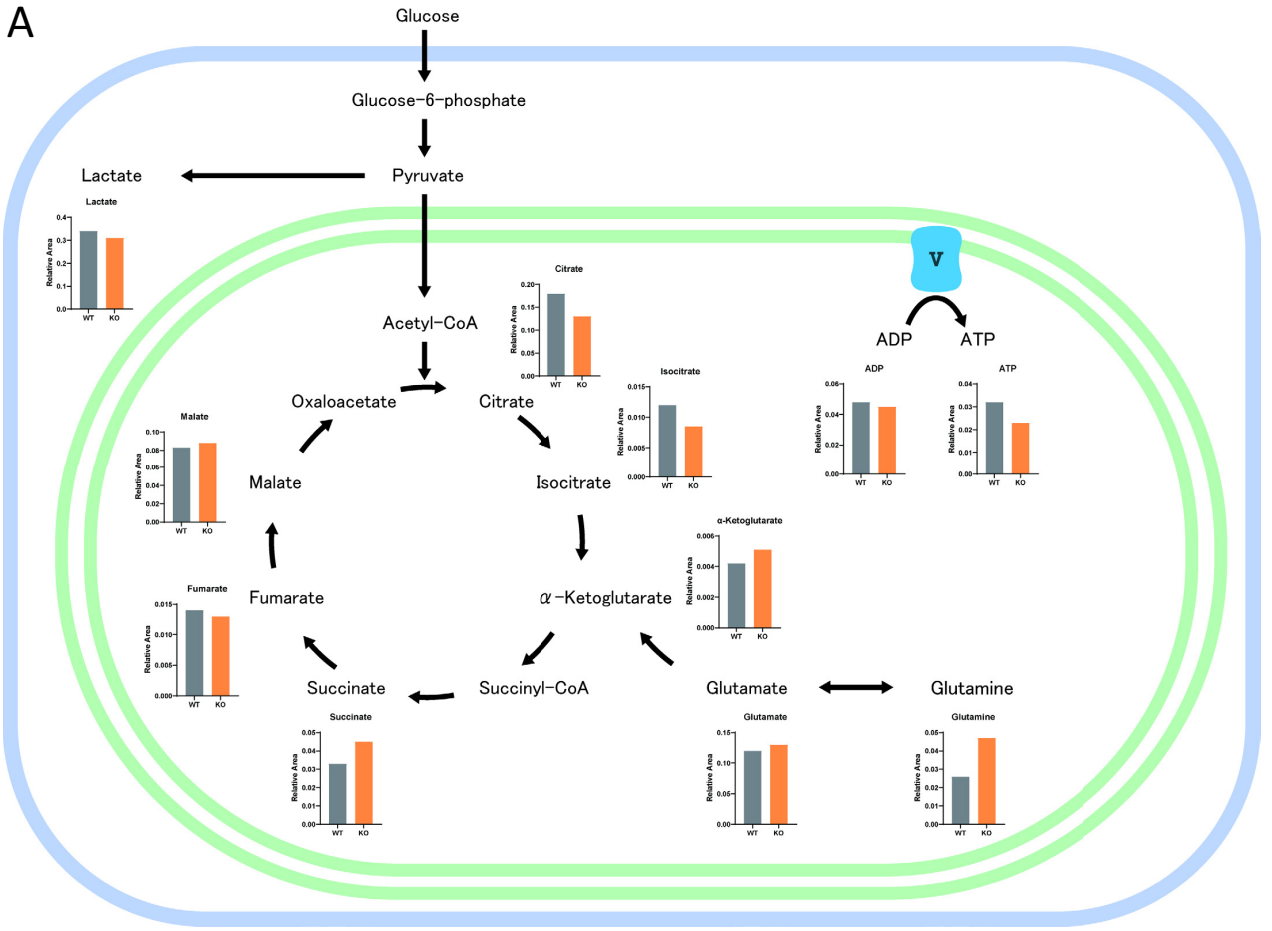

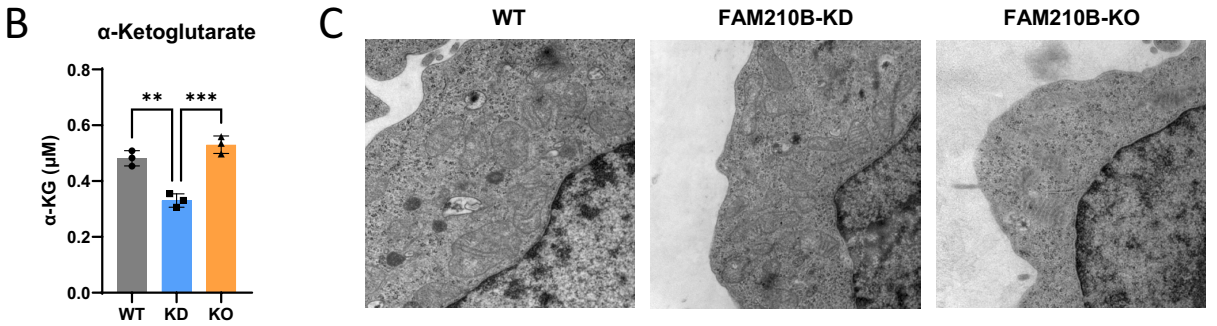

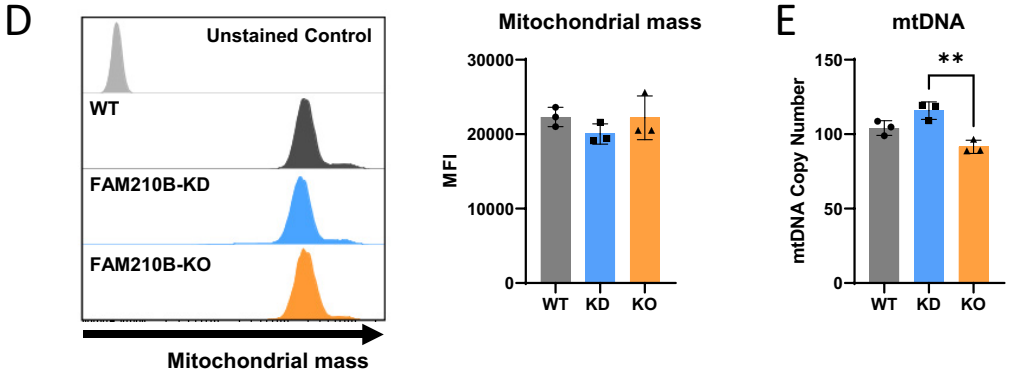

FIG 5 Comprehensive metabolome analysis of FAM210B-depleted HiDEP cells. (A) Summary of metabolome analysis involved in the glycolytic pathway, as well as the TCA (tricarboxylic acid) cycle. (B) Levels of 2-oxoglutaric acid in wild-type, FAM210B-KD, and FAM210B-KO HiDEP cells

(Continued on next page)

(ATP5A) and beta (ATP5B), based on an affinity purification method (Fig. 6C; see also Table S3). Immunoprecipitation of His/biotin-tagged FAM210B using streptavidin beads confirmed interactions with endogenous ATP5A and ATP5B in K562 cells, based on both whole-cell lysate and mitochondrial fraction (Fig. 6D), indicating that FAM210B would interact ATP5A and ATP5B in the mitochondria. While FAM210B depletion did not affect endogenous expression level of ATP5A, ATP5B expression was weakly decreased by the FAM210B knockout (Fig. 6E). We also demonstrated that ATP5B expression was also decreased during erythroid differentiation of HiDEP cells (Fig. 6F). Recently, Yien et al. found that FAM210B could interact with heme biosynthetic enzymes, including ferrochelatase (FECH) and protoporphyrinogen oxidase (PPOX) (13). However, our analysis revealed no interaction with heme biosynthetic enzymes or transporters (i.e., iron, heme, and porphyrin intermediates) that are critical for heme biosynthesis (see Table S3).

In summary, FAM210B was associated with mitochondrial ATP synthases, which indicated it may be involved in mitochondrial energy metabolism.

DISCUSSION

In this study, we generated CRISPR/Cas9-mediated FAM210B-knockdown and FAM210B-knockout HiDEP cells and showed that the potential for erythroid differentiation was more pronounced with *FAM210B* depletion (Fig. 3). Furthermore, both proteomic and metabolome analyses indicated that FAM210B was involved in mitochondrial energy metabolism (Fig. 4 to 6).

Proteomic analysis identified the association of FAM210B with multiple subunits of mitochondrial ATP synthases; for example, FAM210B depletion resulted in decreased oxidative phosphorylation as indicated by decreased OCR (Fig. 4A). Furthermore, the expression level of ATP5B was weakly decreased by FAM210B depletion (Fig. 6E). Since mitochondrial ATP synthase subunits alpha and beta are involved in the F_1F_0-ATP synthase complex located on the mitochondrial inner membrane that belongs to complex V of the mitochondrial chain (31), we speculated that FAM210B might be an adaptor protein that is responsible for maintaining the structure of the F_1F_0-ATP synthase complex for proper ATP production. However, why FAM210B depletion preferentially compromised ATP5B, rather than ATP5A, remained unknown. We demonstrated that the expression of ATP5B protein was moderately decreased during erythroid differentiation of HiDEP cells (Fig. 6F). Because erythroid differentiation levels were almost comparable between wild-type and FAM210B-depleted cells on day 0 (Fig. 1 and 3), we speculate that the weak decrease of ATP5B in the FAM210B knockout cells (Fig. 6E) might not reflect enhanced erythroid differentiation, but might contribute to increased lactate production (Fig. 4D). In addition, decreased expression of *TTC19* (Fig. 1I), which encodes a protein involved in mitochondrial respiratory chain complex III assembly (15), might also contribute to decreased OCR as a result of FAM210B depletion. Furthermore, we also found a decreased NAD^+/NADH redox ratio (Fig. 4E), which reflected impaired mitochondrial complex I activity. Although a direct mechanistic link with FAM210B remains unclear, strong reduction of coenzyme Q10 by FAM210B depletion was observed (99% reduction by FAM210B depletion; see Table S2). Coenzyme Q10 is a lipid-soluble component of the mitochondrial inner membrane, which is critical for carrying electrons from complexes I and II to complex III (32). Thus, we speculate that decreased coenzyme Q10 levels due to FAM210B depletion might impair mitochondrial complex I activity and contribute to decreased OCR. Increased expressions for *TMEM126A* and *NDUFB1*, which is associated with the function of mitochondrial complex I (18, 20), might be compensatory changes by FAM210B depletion (Fig. 1H; see also Table S1).

FIG 5 Legend (Continued)
($n = 3$, means ± the SD; **, $P < 0.01$; ***, $P < 0.001$). (C) Electron microscopy of wild-type, FAM210B-KD, and FAM210B-KO HiDEP cells on day 3 of erythroid differentiation. (D) Total amounts of mitochondria in wild-type, FAM210B-KD, and FAM210B-KO HiDEP cells on day 3 of erythroid differentiation. The left and right panels indicate representative data and the average of three independent experiments, respectively (means ± the SD). (E) Quantification of mtDNA in wild-type, FAM210B-KD, and FAM210B-KO HiDEP cells ($n = 3$, means ± the SD; **, $P < 0.01$).

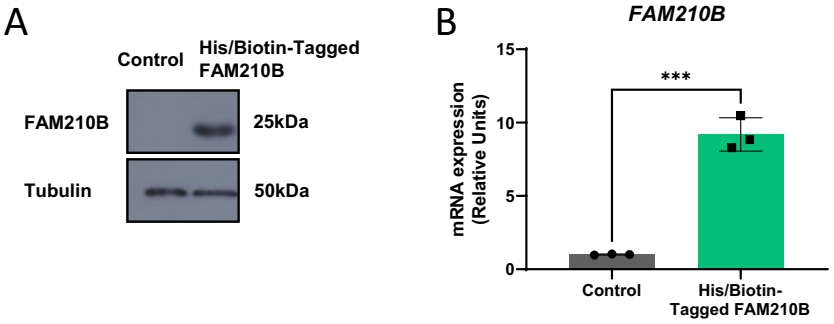

C

	Experiment1		Experiment2	
	Control	His/Biotin-Tagged FAM210B	Control	His/Biotin-Tagged FAM210B
FAM210B	0	32	0	24
ATP synthase subunit alpha, mitochondrial	1	15	2	14
ATP synthase subunit beta, mitochondrial	2	11	1	14
ATP synthase subunit gamma, mitochondrial	1	2	0	2
ATP synthase subunit delta, mitochondrial	0	1	-	-
Lamin-B1	2	16	2	23
Heterogeneous nuclear ribonucleoprotein H	2	18	1	13
Vimentin	1	20	1	21

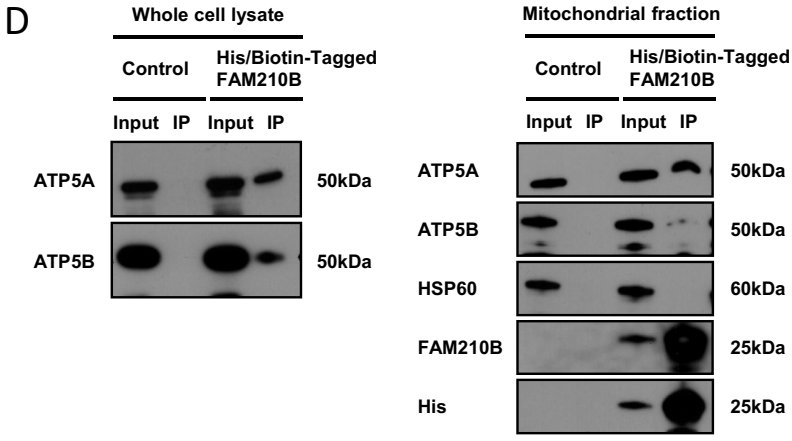

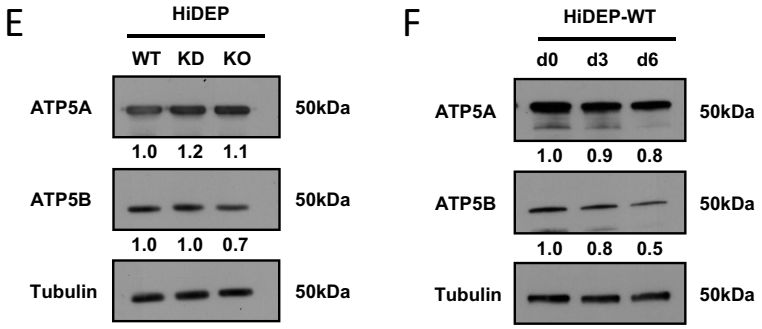

FIG 6 Proteomic analysis to identify FAM210B-interacting proteins. (A) Western blot of proteins from lysates of K562 cells and K562 cells stably expressing His/biotin-tagged FAM210B probed with monoclonal anti-His. Blots probed with anti-α-tubulin were used as loading controls. (B) Quantitative RT-PCR analysis (B) of *FAM210B* mRNA in wild-type and FAM210B-overexpressing K562 cells, all normalized to *GAPDH* (n = 3, means $\pm$ the SD; ***, $P < 0.001$). (C) Representative data for affinity purification of FAB210B and FAB210B-interacting proteins from K562 cells stably expressing FAM210B. Ratios presented indicate relative enrichment of each peptide in cells overexpressing FAM210B (average of two independent experiments). (D) Immunoprecipitation of His/Biotin-tagged FAM210B in K562 cells. Western blots for ATP synthase alpha (ATP5A) and beta (ATP5B) are shown. The left and right panels indicate the immunoprecipitation analysis based on the whole-cell lysate and the mitochondrial

(Continued on next page)

During erythroid differentiation of HiDEP cells, we found decreased OCR (Fig. 2D). Thus, it may be possible that decreased OCR, and several mitochondrial phenotypes observed by FAM210B knockout (Fig. 4) are likely be due to the enhanced differentiation in the FAM210B knockout cells. However, based on the comparable differentiation levels between wild-type and FAM210B-depleted cells on day 0 (Fig. 1 and 3), we speculate that enhanced lactate levels in the culture media (Fig. 4D) might be caused by mitochondrial dysfunction through FAM210B defect, rather than reflecting enhanced erythroid differentiation status in FAM210B-depleted cells.

Despite decreased OCR due to FAM210B depletion (Fig. 4A), ATP production (Fig. 4B) was not obviously decreased by FAM210B depletion. We therefore speculated that a shift toward anaerobic glycolysis might compensate for compromised ATP production by oxidative phosphorylation, as indicated by increased lactate levels in the culture supernatant (Fig. 4D). However, intracellular lactate levels were not significantly increased or marginally increased in the FAM210B knockout cells (Fig. 4H and 5A). Though the underlying mechanisms that cause the discrepancy remains unknown, we speculate that FAM210B depletion might weakly induce lactate production by inducing a shift toward anaerobic glycolysis, which would gradually accumulate in the culture media. On the other hand, while metabolites derived from acetyl-CoA, such as citric acid and isocitric acid, were decreased with FAM210B depletion, the 2-OG level was almost unchanged (Fig. 5B; see also Table S2). In addition to isocitric acid, glutamine could be an important source for the generation of 2-OG (Fig. 5A) and is involved in several biological processes, such as cell growth, lipid metabolism, and insulin secretion (33). In later stages of erythropoiesis, exogenous glutamine, rather than the TCA cycle intermediates, could provide carbons for succinyl-CoA for heme biosynthesis (34). Intriguingly, glutamine levels were obviously enhanced with FAM210B depletion (1.8-fold increase by FAM210B KO; Fig. 5A; see also Table S2). Thus, in consideration of our observations that erythroid differentiation was more pronounced in FAM210B-depleted HiDEP cells (Fig. 3), we speculated that the glutamine supply might compensate for the decreased TCA cycle intermediates (Fig. 7). Nevertheless, the molecular mechanism by which glutamine levels could be enhanced by FAM210 knockout remained elusive in the present study. Thus, further analyses are required.

There are several published reports that demonstrated an association between mitochondrial ATP levels and erythroid differentiation: specifically, depletion of the mitochondrial ATP transporter, *Ant2*, and impaired erythropoiesis in mice (35). In addition, increased oxidative phosphorylation in response to *ATG7* knockdown induced erythroid differentiation of $CD34^+$ chronic myeloid leukemia cells (36). These reports suggested that ATP production might have a positive impact on erythroid differentiation. In contrast, depletion of mitochondrial ATPase inhibitory factor 1 (*Atpif1*) results in inhibition of heme biosynthesis and erythroid differentiation (37), which are findings that are consistent with our observations. In addition to the role of mitochondrial ATP production on erythroid differentiation, Richard and colleagues revealed that an increase in lactate levels could serve as an important driving force toward erythroid differentiation (38). Similarly, we found increased lactate levels in the culture media as a result of FAM210B depletion (Fig. 4D), which might represent a shift toward glycolytic metabolism in response to reduced OCR (39), or it may be partly related to reduced complex I activity, as indicated by a decreased NAD^+/NADH redox ratio (Fig. 4E). Therefore, we speculated that dynamic changes in the glycolytic metabolism *versus* oxidative phosphorylation that are involved in erythroid differentiation might be dependent on the specific context and microenvironment in which these events take place. Although the total amount of mitochondria was not affected (Fig. 1D and Fig. 5C to E), we observed

FIG 6 Legend (Continued)
fraction, respectively. (E) Western blot for ATP5A and ATP5B in wild-type and *FAM210B*-KO HiDEP cells. ATP5A and ATP5B protein signals were quantified and normalized to that of α-tubulin. The result was representative of two independent experiments. (F) Western blot for ATP5A and ATP5B in days 0, 3, and 6 of erythroid differentiation of wild-type HiDEP cells. ATP5A and ATP5B protein signals were quantified and normalized to that of α-tubulin. The result was representative of two independent experiments.

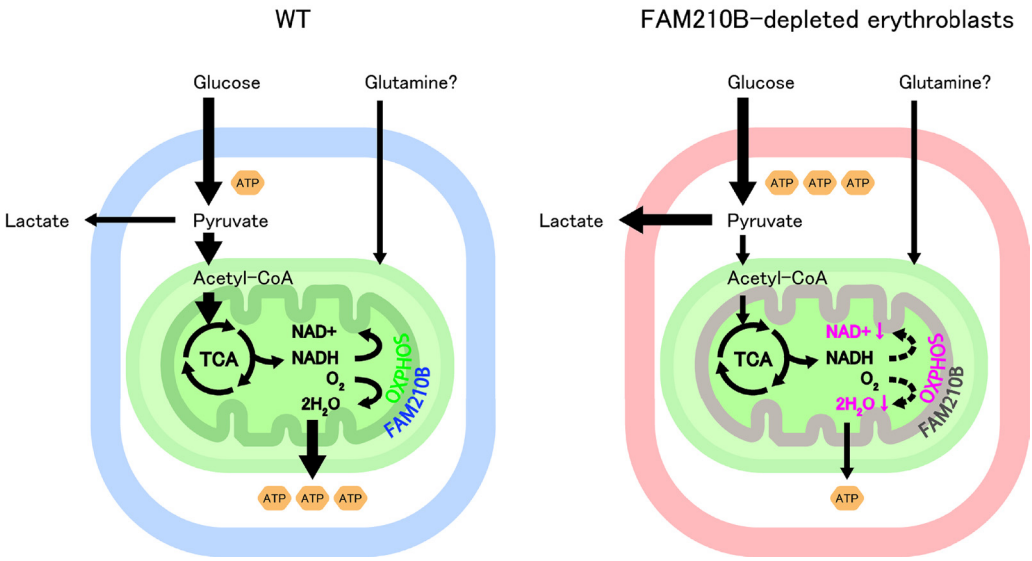

FIG 7 Proposed model for the role of FAM210B in promoting erythroid differentiation. The scheme indicated glucose and mitochondrial energy metabolism in wild-type (left) and FAB210B-depleted (right) erythroblasts. Our results suggested that FAM210B depletion resulted in decreased ATP production by oxidative phosphorylation (OXPHOS), while increased lactate levels by anaerobic glycolysis were observed; both might contribute to promotion of erythroid differentiation by affecting the mitochondrial energy metabolism.

smaller mitochondrial sizes with FAB210B depletion, which might be associated with reduced mitochondrial respiratory activity or simply reflect greater promotion of erythroid differentiation (40). Nevertheless, our results showed that FAM210B depletion resulted in increased lactate levels and decreased OCR contributed to stimulation of erythroid differentiation (Fig. 7).

In a previous study, we demonstrated that small interfering RNA (siRNA)-mediated transient knockdown of *FAM210B* in undifferentiated HiDEP cells resulted in moderate downregulation of *ALAS2*, *HBG*, and *HBA* (12). In addition, a recent study indicated that antisense morpholino-mediated knockdown in zebrafish produced an anemic phenotype (13). Because HiDEP cells are derived from iPS cells (23), we need to consider the possibility that FAM210B depletion might result in mitochondrial metabolic reprogramming, which ultimately favors erythroid differentiation. This interpretation is supported, at least in part, by the observation that stable FAM210B depletion resulted in altered expression of mitochondrial genes (i.e., *TTC19*, *AARS2*, *CLIC1*, *MRPL53*, *TMEM126A*, *CYC1*, *NDUFB1*, *PDHX*, and *PANK2*; Fig. 1H and I; see also Table S1). As such, the role of FAM210B should be evaluated in other cell types, such as human cord blood $CD34^+$ hematopoietic progenitors (HUDEP-2) (23) or primary erythroblasts. In addition, we recognize that erythroid differentiation was induced by coculturing with OP9 cells with the addition of ferrous iron (24). This may result in compensation for the impaired iron import observed in response to FAM210B depletion. It is also possible that the erythroid differentiation protocols used in this study might only be effective when targeting FAM210B-depleted HiDEP cells. Additional means of promoting erythroid differentiation should be explored. Further studies of other cell types, including different culture protocols, are required to address this question.

In this study, we generated both *FAM210B*-knockdown and -knockout HiDEP cell lines (Fig. 1) with CRISPR/Cas9-mediated gene editing and confirmed the phenotypic changes were mostly FAM210B knockdown efficiency dependent (Fig. 3 to 5). However, to completely rule out the possibility of an off-target effect, it would be desirable to establish FAM210B-disrupted clones based on different guide RNA sequences or to check whether the phenotypic changes by FAM210B depletion could be restored by exogenous

FAM210B reconstitution in the knockout clone. This issue would be a limitation of the study to be addressed in the future.

The human *FAM210B* gene is located on the long arm of chromosome 20. Deletion of this region (del 20q) has been observed in 3 to 7% of patients with myelodysplastic syndrome (MDS) (41). Interestingly, individuals diagnosed with del 20q MDS showed increased reticulocyte counts (42). Although the contribution of FAM210B to augmented erythropoiesis remains unknown, this evidence supports our observations and suggests the involvement of FAM210B in human disease.

In summary, we characterized the actions of FAM210B in erythroid progenitor cells. Specifically, FAM210B contributes prominently to erythroid differentiation by regulating mitochondrial energy metabolism, through interacting with multiple subunits of mitochondrial ATP synthases. Our results provide insights into the pathophysiology of underlying states of decreased erythropoiesis.

MATERIALS AND METHODS

Cell culture. All cells were cultured in a humidified incubator at 37°C with a 5% carbon dioxide atmosphere. Human K562 erythroleukemia cell lines were maintained in RPMI 1640 medium containing 10% fetal bovine serum (FBS; Life Technologies) and 1% penicillin-streptomycin (Life Technologies). The HEK293T cell line (ATCC CRL-1573) was maintained in Dulbecco modified Eagle medium containing 10% FBS (Life Technologies) and 1% penicillin-streptomycin (Life Technologies). Human induced pluripotent stem (iPS) cell-derived erythroid progenitors (HiDEPs) (23) were cultured in StemSpan serum-free expansion medium (SFEM; Stem Cell Technologies, Vancouver, BC, Canada) containing 3 U/mL erythropoietin (EPO; Kyowa Hakko Kirin, Tokyo, Japan), 1 μg/mL doxycycline (DOX; Sigma-Aldrich Corp., St. Louis, MO), and 1 μM dexamethasone (DEX; Sigma-Aldrich Corp.). OP9 cells were cultured in α-minimum essential medium (α-MEM; Gibco, Grand Island, NY) supplemented with 20% FBS (Life Technologies) and 1% penicillin-streptomycin (Life Technologies).

To induce erythroid differentiation of HiDEP cells, we applied coculture system with OP9 stromal cells, obtained from the American Type Culture Collection (Manassas, VA). At 48 h before coculture, 50,000 OP9 cells were seeded onto a 10-cm dish in Iscove modified Dulbecco medium (IMDM; Sigma-Aldrich Corp.) supplemented with 20% FBS, 1% penicillin-streptomycin. Then, the 50,000 HiDEP cells were seeded onto the OP9 cells in IMDM supplemented with 20% FBS, insulin-transferrin-selenium (Gibco), 50 μg/mL L-ascorbic acid 2-phosphate (Sigma-Aldrich Corp.), 0.45 mM 1-thioglycerol (MTG; Sigma-Aldrich Corp.), 1% penicillin-streptomycin, 3 IU/mL EPO, 1 μg/mL DOX, and 1 μM DEX (24). Erythroid differentiation was conducted for up to 6 days.

Generation of FAM210B knockdown and knockout cell lines using the CRISPR/Cas9 system. The target sequence that was used to disrupt the human *FAM210B* gene was 5′-GATTGCATAGGCCACCACGA-3′, which was located at exon 3 of the protein coding sequence. The PrecisionX LentiCas9 SmartNuclease System (System Bioscience, Palo Alto, CA) was used to introduce a mutation into HiDEP cells, as described previously (24). Briefly, we first established HiDEP cells stably expressing Cas9 nuclease based on Cas9 and Nickase lentivector. Subsequently, the gRNA expressing lentiviral plasmid (Cas9 SmartNuclease vector) containing target sequence against *FAM210B* was transduced into the Cas9-expressing HiDEP cells. Each lentiviral vector was cotransfected with psPAX (Addgene, catalog no. 12260) and pMD2.G (Addgene, catalog no. 12259) into HEK293 cells for the production of lentiviral particle. Clonal cell lines were isolated by serial dilution and mutations were detected by direct sequencing of PCR amplicons. The experimental protocol was approved by the Committee for Safe Handling of Living Modified Organisms of Tohoku University Graduate School of Medicine.

Primers. Primer sequences that were used to detect human FAM210B mRNA (mRNA) were as follows: human *FAM210B*, forward (5′-CCTTGGGCATATTTTACATGGT-3′) (located on exon 2) and reverse (5′-AAACAGCTTGTGGATTGCATAG-3′) (located on exon 3); human *TTC19*, forward (5′-AAGCGAGCCAAGTTGAGCAT-3′) and reverse (5′-GCATTTTCAAGCTGACCCCG-3′); human *ASNS*, forward (5′-CTGCACGCCCTCTATGACAA-3′) and reverse (5′-GGAGTCCAAGCCCCCTGATA-3′); human *AKR1B1*, forward (5′-CTACCTTATTCACTGGCCGACT-3′) and reverse (5′-GTTGGAGATGCCAATAGCTTTC-3′); human *SLC2A1*, forward (5′-CAGTTTGGCTACAACACTGGAG-3′) and reverse (5′-GGACCCATGTCTGGTTGTAGA-3′); human *MPC1*, forward (5′-GGACTATGTCCGAAGCAAGG-3′) and reverse (5′-AAATGTCATCCGCCCACTGA-3′); human *MPC2*, forward (5′-TGTGTGCTGGATTGGCTGAT-3′) and reverse (5′-CCAAATAAACCCTGTAGCCATCAA-3′); and human *SLC16A1*, forward (5′-CATGCCACCACCAGCGAAG-3′) and reverse (5′-TGACAAGCAGCCACCAACAATC-3′). All other primers that were used were described previously (5, 43).

Genome analysis. Sanger sequence was conducted based on genome DNA derived from wild-type and FAM210B-depleted K562 cells, using ABI3730xl DNA analyzer and ABI BigDye terminator cycle sequencing kit (Applied Biosystems, Foster City, CA). Genomic DNA was extracted with a DNeasy blood and tissue kit (Qiagen, Valencia, CA).

Cytospin. Cultured cells were centrifuged at 500 rpm (rpm) for 3 min and placed onto glass slides using a Shandon Cytospin 4 Cytocentrifuge (Thermo, Pittsburgh, PA). The cells were subsequently analyzed with microscopy after staining with May-Grünwald Giemsa (Merck KGaA, Darmstadt, Germany).

Gene transfer and vectors. The human *FAM210B* coding sequence was cloned into His/Biotin-Tagged pQCX retroviral vectors. The retroviral vector and the *env* (envelope glycoprotein) gene from the

vesicular stomatitis virus (VSV-G) were cotransfected into target cells using PLAT-GP Packaging Cell Lines with FuGene HD (Promega). After spin infection into K562 cells at 3,400 rpm for 2 h, the cells were cultured with medium containing 1 μg/mL Puromycin (Sigma) for selection of the transduced cells.

Mass spectrometry. Fifty million K562 cells that stably expressed the FAM210B-HisBio protein were harvested and then lysed in 1.5 mL of the lysis buffer consisting of 50 mM Tris-HCl (pH 7.4), 150 mM NaCl, 0.3% (wt/vol) NP-40, protease inhibitor complete (Roche), and PhosStop (Roche). After centrifugation at 15,000 rpm for 5 min, the cleared lysate was mixed with Dynal streptavidin beads (20 μL of slurry was equilibrated by the lysis buffer three times) with rotation for 1.5 h. The beads were washed three times using a lysis buffer and the isolated proteins were eluted twice using an elution buffer (50 mM Tris-HCl [pH 8], 0.2 M NaCl, 2% sodium dodecyl sulfate [SDS], and 1 mM biotin). The proteins were separated with 5 to 20% SDS-polyacrylamide gels (Oriental Instruments) and then stained with Coomassie brilliant blue staining. Every lane was divided into three sections and these gel pieces were cut out. After the samples were destained and dehydrated with acetonitrile, they were reduced with 10 mM dithiothreitol in 25 mM ammonium bicarbonate and then alkylated with 55 mM acrylamide in 25 mM ammonium bicarbonate. Every sample was subsequently digested with 30 ng of trypsin (Promega) at 37°C overnight. The resulting tryptic peptides were extracted three times with an elution solution composed of 75% acetonitrile and 1% formic acid. Finally, the sample volume was reduced with a SpeedVac. The samples were subjected to liquid chromatography-tandem mass spectrometry (LC-MS/MS) using an Orbitrap Fusion mass spectrometer equipped with an Easy-nLC 1000 HPLC system (Thermo Fisher Scientific). Next, the peptides were separated using a C_{18} tip column (75-μm [inner diameter] $\times$ 10-cm L; Nikkyo Technos) at a 300-nL/min flow rate with a 40-min gradient, which was generated by solvent A (0.1% formic acid in water; Thermo Fisher Scientific) and solvent B (0.1% formic acid in acetonitrile; Thermo Fisher Scientific). The protocol was 5% B to 25% B in 31 min, to 35% B in 36 min, to 95% B in 38 min, to 95% B from 38 to 39 min, and finally to 5% B in 40 min. MS^1 scans from m/z = 321 to 1,500 were performed with an Orbitrap mass spectrometer with the resolution set to 120,000 and lock masses at m/z = 445.12003 and 391.28429. This was followed by the acquisition of collision-induced dissociation (CID)-MS^2 scans in an ion trap. The settings for the MS^2 scans were as follows: intensity threshold = 1,000, charge states = +2 to +6, isolation width = 1.2 m/z, AGC target = 5,000, maximum ion injection time = 50 ms, normalized collision energy = 35%, and dynamic exclusion enabled with a 30-s exclusion duration. The MS/MS cycle time was set to 4 s. The MS/MS data were acquired over 46 min after the LC gradient began. Every three raw data files of the samples derived from the same SDS-PAGE lane were converted to a single mascot generic format (mgf) file with Proteome Discoverer software (v1.4; Thermo Fisher Scientific). Protein identification was performed using the MASCOT search engine (v2.6.0; Matrix Science) by searching the human protein database in Swiss-Prot (Jan. 2018) and a "lab made" protein list, including common contaminating proteins. A maximum of three trypsin miscleavages was allowed. Propionamidated cysteine (+71.0371) was set as a fixed modification, and protein N-terminal acetylation (+42.0106 Da) and oxidation of methionine (+15.9949 Da) were selected as variable modifications. The peptide mass tolerance and MS/MS tolerance were set at 5 ppm and 0.5 Da, respectively (44).

Real-time quantitative RT-PCR analysis. Total RNA was purified with TRIzol (Invitrogen). cDNAs were synthesized from purified total RNA using ReverTra Ace qPCR RT Master Mix (Toyobo, Tokyo, Japan). A QuantiTect SYBR green PCR kit (Qiagen, Hilden, Germany) was used for mRNA quantification. PCR product abundance was normalized relative to amplified *GAPDH* mRNA (43).

Quantification of mitochondrial DNA. To quantify mitochondrial DNA amount, human mitochondrial DNA (mtDNA) Monitoring Primer set and MightyAmp for Real Time (TB Green Plus; TaKaRa Bio, Inc., Otsu, Japan) were used.

Microarray analysis. Human Oligo chip 25k (Toray, Tokyo, Japan) was used for expression profiling (43). Gene ontology (GO) analysis was performed using Genecoids (https://www.hsls.pitt.edu/obrc/index.php?page=URL1253281518).

Western blotting. Western blot analyses were performed as described previously (5, 43). Dynabeads M-280 streptavidin (Thermo Fisher Scientific, Waltham, MA) was used to purify biotinylated FAM210B-interacting proteins. For separation of mitochondrial fraction, Mitochondrial isolation kit for Cultured Cells (Thermo Fisher Scientific) was used. Anti-ATP5A, -ATP5B, and -HSP60 antibodies were obtained from Proteintech (Rosemont, IL) and Sigma, respectively. Anti-α-tubulin antibody (CP06) was obtained from Calbiochem (San Diego, CA). The anti-FAM210B antibody was obtained from Atlas Antibodies (Bromma, Sweden). The proteins were measured with ECL-Plus (Thermo Fisher Scientific) and CL-X Posure Film (Thermo Scientific, Rockford, IL). For the detection of FAM210B protein, SuperSignal West Femto Maximum Sensitivity Substrate, SuperSignal Western Blot Enhancer, and SuperBlock (TBS) blocking buffer (Thermo Fisher Scientific) were used. Each band was quantified with ImageJ software (http://rsbweb.nih.gov/ij/). For calculating relative intensity, control samples (wild-type) were set to 1.

Flow cytometry. The cells were washed and resuspended in phosphate-buffered saline containing 3% FBS, followed by incubation with fluorescence-conjugated antibodies specific for CD71 (clone M-A712, allophycocyanin conjugated), and CD235a (clone GA-R2, BV421 conjugated) (Becton Dickinson, Franklin Lakes, NJ). Propidium iodide (Thermo Fisher Scientific) was used to mark dead cells. Data were acquired with a FACS Aria II (Becton Dickinson) and analyzed using FlowJo software (TreeStar, Ashland, OR).

Intracellular heme concentrations. The intracellular heme concentration was quantified using a spectrofluorometer (RF-5300PC; Shimadzu, Kyoto, Japan), as described previously (45). Cells were harvested and centrifuged at 300 $\times$ *g* for 5 min. Cell pellets were suspended in 2 M oxalic acid (Sigma-Aldrich) and boiled at 100°C for 30 min to dissociate protoporphyrin IX and iron from heme. Subsequently, fluorescence for protoporphyrin IX was measured with excitation at 400 nm and emission at 662 nm.

Electron microscopy. HiDEP cells were fixed with 2% paraformaldehyde and 2.5% glutaraldehyde in 0.1 M cacodylate buffer, as described previously (24). The cells were then postfixed in 1% osmium tetroxide for 30 min at 4°C, rinsed in 0.1 M cacodylate buffer containing 8% sucrose, dehydrated in a graded series of alcohol and propylene oxide, and finally embedded in epoxy resin. Ultrathin (75 nm) sections were prepared with an ultramicrotome (UC-7; Leica, Heerbrugg, Switzerland), and the sections were stained with uranyl acetate and lead citrate before viewing with electron microscopy (H-7600; Hitachi, Tokyo, Japan).

Evaluation of mitochondrial mass. To assess mitochondrial mass, MitoBright LT Deep Red (Dojindo Molecular Technologies, Inc., Kumamoto, Japan) was used.

Evaluation of the oxygen consumption rate. A PHERAstar FSX microplate reader (BMG Labtech, Germany) and MitoXpress Xtra (Agilent) were used to evaluate the oxygen consumption rate, according to the manufacturer's protocol.

Global metabolite analysis. Global metabolite analysis of control and FAM210B-knockout HiDEP cells was performed by Human Metabolite Technologies (Tokyo, Japan) as a contracted service. We prepared the samples for both CE (capillary electrophoresis)-TOFMS (time-of-flight mass spectrometry) and LC (Liquid Chromatography)-TOFMS analyses. For preparation of CE-TOFMS samples, 5 million cells were washed with 10 mL of 5% mannitol solution, then treated with 800 μL of methanol and vortexed for 30 s. The cell extract was treated with 550 μL of internal standard solution (provided by Human Metabolite Technologies) and vortexed for 30 s. After centrifugation at 2,300 $\times$ *g* for 5 min at 4°C, the upper layer was collected and centrifugally filtered through a Millipore 5-kDa cutoff filter at 9,100 $\times$ *g* for 120 min at 4°C to remove proteins. The filtrate was centrifugally concentrated and resuspended with 800 μL of water. For preparation of LC-TOFMS samples, 5 million cells were washed with 10 mL of 5% mannitol solution and subsequently centrifuged to completely remove mannitol. Then, the cells were treated with the metabolite extract ethanol solution containing internal standard solution (provided by Human Metabolite Technologies). All samples were measured and analyzed by Human Metabolite Technologies.

Measurement of mitochondrial metabolism. Glucose consumption and lactate production were measured with a glucose assay kit and lactate assay kit, respectively (Dojindo Molecular Technologies, Inc., Kumamoto, Japan). The redox state of the NAD^+/NADH ratio was evaluated with an NAD/NADH assay kit (Dojindo Molecular Technologies, Inc., Kumamoto, Japan). The ATP level was measured with a luminescent ATP detection kit (Abcam, Cambridge, UK). To measure lactate levels in the culture supernatant, samples were obtained after 18 h of culture.

Statistics. Statistical significance was assessed with a two-tailed Student *t* test or one-way analysis of variance with Tukey's multiple-comparison tests.

SUPPLEMENTAL MATERIAL

Supplemental material is available online only.

SUPPLEMENTAL FILE 1, XLSX file, 0.1 MB.

SUPPLEMENTAL FILE 2, XLSX file, 0.1 MB.

SUPPLEMENTAL FILE 3, XLSX file, 0.8 MB.

ACKNOWLEDGMENTS

We acknowledge the members of the Biomedical Research Core of Tohoku University School of Medicine for their support.

This study was supported by The Ichiro Kanehira Foundation (T.F.).

All authors declare there are no conflicts of interest.

C.S., T.F., H.S., K.O. (Ono), and K.S. performed the experiments and analyzed the data. T.F., H.K., K.O. (Onodera), S.I., N.F., Y.O., H.Y., Y.N., K.I., and H.H. contributed samples/reagents. T.F. and H.H. wrote the paper.

REFERENCES

1. Bresnick EH, Lee HY, Fujiwara T, Johnson KD, Keles S. 2010. GATA switches as developmental drivers. J Biol Chem 285:31087–31093. https://doi.org/10.1074/jbc.R110.159079.
2. Fujiwara T. 2017. GATA transcription factors: basic principles and related human disorders. Tohoku J Exp Med 242:83–91. https://doi.org/10.1620/tjem.242.83.
3. Ling T, Crispino JD. 2020. GATA1 mutations in red cell disorders. IUBMB Life 72:106–118. https://doi.org/10.1002/iub.2177.
4. Katsumura KR, Bresnick EH, GATA factor mechanisms group. 2017. The GATA factor revolution in hematology. Blood 129:2092–2102. https://doi.org/10.1182/blood-2016-09-687871.
5. Fujiwara T, O'Geen H, Keles S, Blahnik K, Linnemann AK, Kang Y-A, Choi K, Farnham PJ, Bresnick EH. 2009. Discovering hematopoietic mechanisms through genome-wide analysis of GATA factor chromatin occupancy. Mol Cell 36:667–681. https://doi.org/10.1016/j.molcel.2009.11.001.
6. Yu M, Riva L, Xie H, Schindler Y, Moran TB, Cheng Y, Yu D, Hardison R, Weiss MJ, Orkin SH, Bernstein BE, Fraenkel E, Cantor AB. 2009. Insights into GATA-1-mediated gene activation versus repression via genome-wide chromatin occupancy analysis. Mol Cell 36:682–695. https://doi.org/10.1016/j.molcel.2009.11.002.
7. Soler E, Andrieu-Soler C, de Boer E, Bryne JC, Thongjuea S, Stadhouders R, Palstra RJ, Stevens M, Kockx C, van IJcken W, Hou J, Steinhoff C, Rijkers E, Lenhard B, Grosveld F. 2010. The genome-wide dynamics of the binding of Ldb1 complexes during erythroid differentiation. Genes Dev 24:277–289. https://doi.org/10.1101/gad.551810.
8. Gonzalez-Ibanez AM, Ruiz LM, Jensen E, Echeverria CA, Romero V, Stiles L, Shirihai OS, Elorza AA. 2020. Erythroid differentiation and heme

biosynthesis are dependent on a shift in the balance of mitochondrial fusion and fission dynamics. Front Cell Dev Biol 8:592035. https://doi.org/10.3389/fcell.2020.592035.
9. Liao R, Bresnick EH. 2022. Heme as a differentiation-regulatory transcriptional cofactor. Int J Hematol 116:174–181. https://doi.org/10.1007/s12185-022-03404-x.
10. Chiabrando D, Mercurio S, Tolosano E. 2014. Heme and erythropoiesis: more than a structural role. Haematologica 99:973–983. https://doi.org/10.3324/haematol.2013.091991.
11. Sandoval H, Thiagarajan P, Dasgupta SK, Schumacher A, Prchal JT, Chen M, Wang J. 2008. Essential role for Nix in autophagic maturation of erythroid cells. Nature 454:232–235. https://doi.org/10.1038/nature07006.
12. Kondo A, Fujiwara T, Okitsu Y, Fukuhara N, Onishi Y, Nakamura Y, Sawada K, Harigae H. 2016. Identification of a novel putative mitochondrial protein FAM210B associated with erythroid differentiation. Int J Hematol 103:387–395. https://doi.org/10.1007/s12185-016-1968-4.
13. Yien YY, Shi J, Chen C, Cheung JTM, Grillo AS, Shrestha R, Li L, Zhang X, Kafina MD, Kingsley PD, King MJ, Ablain J, Li H, Zon LI, Palis J, Burke MD, Bauer DE, Orkin SH, Koehler CM, Phillips JD, Kaplan J, Ward DM, Lodish HF, Paw BH. 2018. FAM210B is an erythropoietin target and regulates erythroid heme synthesis by controlling mitochondrial iron import and ferrochelatase activity. J Biol Chem 293:19797–19811. https://doi.org/10.1074/jbc.RA118.002742.
14. Sun S, Liu J, Zhao M, Han Y, Chen P, Mo Q, Wang B, Chen G, Fang Y, Tian Y, Zhou J, Ma D, Gao Q, Wu P. 2017. Loss of the novel mitochondrial protein FAM210B promotes metastasis via PDK4-dependent metabolic reprogramming. Cell Death Dis 8:e2870. https://doi.org/10.1038/cddis.2017.273.
15. Ghezzi D, Arzuffi P, Zordan M, Da Re C, Lamperti C, Benna C, D'Adamo P, Diodato D, Costa R, Mariotti C, Uziel G, Smiderle C, Zeviani M. 2011. Mutations in TTC19 cause mitochondrial complex III deficiency and neurological impairment in humans and flies. Nat Genet 43:259–263. https://doi.org/10.1038/ng.761.
16. Götz A, Tyynismaa H, Euro L, Ellonen P, Hyötyläinen T, Ojala T, Hämäläinen RH, Tommiska J, Raivio T, Oresic M, Karikoski R, Tammela O, Simola KO, Paetau A, Tyni T, Suomalainen A. 2011. Exome sequencing identifies mitochondrial alanyl-tRNA synthetase mutations in infantile mitochondrial cardiomyopathy. Am J Hum Genet 88:635–642. https://doi.org/10.1016/j.ajhg.2011.04.006.
17. Yang JY, Jung JY, Cho SW, Choi HJ, Kim SW, Kim SY, Kim HJ, Jang CH, Lee MG, Han J, Shin CS. 2009. Chloride intracellular channel 1 regulates osteoblast differentiation. Bone 45:1175–1185. https://doi.org/10.1016/j.bone.2009.08.012.
18. D'Angelo L, Astro E, De Luise M, Kurelac I, Umesh-Ganesh N, Ding S, Fearnley IM, Gasparre G, Zeviani M, Porcelli AM, Fernandez-Vizarra E, Iommarini L. 2021. NDUFS3 depletion permits complex I maturation and reveals TMEM126A/OPA7 as an assembly factor binding the ND4-module intermediate. Cell Rep 35:109002. https://doi.org/10.1016/j.celrep.2021.109002.
19. Sato A, Takagi K, Miki Y, Yoshimura A, Hara M, Ishida T, Sasano H, Suzuki T. 2019. Cytochrome c1 as a favorable prognostic marker in estrogen receptor-positive breast carcinoma. Histol Histopathol 34:1365–1375. https://doi.org/10.14670/HH-18-130.
20. Ellinger J, Poss M, Brüggemann M, Gromes A, Schmidt D, Ellinger N, Tolkach Y, Dietrich D, Kristiansen G, Müller SC. 2017. Systematic expression analysis of mitochondrial complex I identifies NDUFS1 as a biomarker in clear-cell renal-cell carcinoma. Clin Genitourin Cancer 15:e551–e562. https://doi.org/10.1016/j.clgc.2016.11.010.
21. Schiff M, Miné M, Brivet M, Marsac C, Elmaleh-Bergés M, Evrard P, Ogier de Baulny H. 2006. Leigh's disease due to a new mutation in the PDHX gene. Ann Neurol 59:709–714. https://doi.org/10.1002/ana.20818.
22. Munshi MI, Yao SJ, Ben Mamoun C. 2022. Redesigning therapies for pantothenate kinase-associated neurodegeneration. J Biol Chem 298:101577. https://doi.org/10.1016/j.jbc.2022.101577.
23. Kurita R, Suda N, Sudo K, Miharada K, Hiroyama T, Miyoshi H, Tani K, Nakamura Y. 2013. Establishment of immortalized human erythroid progenitor cell lines able to produce enucleated red blood cells. PLoS One 8:e59890. https://doi.org/10.1371/journal.pone.0059890.
24. Saito K, Fujiwara T, Hatta S, Morita M, Ono K, Suzuki C, Fukuhara N, Onishi Y, Nakamura Y, Kawamata S, Shimizu R, Yamamoto M, Harigae H. 2019. Generation and molecular characterization of human ring sideroblasts: a key role of ferrous iron in terminal erythroid differentiation and ring sideroblast formation. Mol Cell Biol 39:e00387-18. https://doi.org/10.1128/MCB.00387-18.
25. Garcia-Santos D, Schranzhofer M, Horvathova M, Jaberi MM, Bogo Chies JA, Sheftel AD, Ponka P. 2014. Heme oxygenase 1 is expressed in murine erythroid cells where it controls the level of regulatory heme. Blood 123:2269–2277. https://doi.org/10.1182/blood-2013-04-496760.
26. Halestrap AP. 2013. The SLC16 gene family: structure, role, and regulation in health and disease. Mol Aspects Med 34:337–349. https://doi.org/10.1016/j.mam.2012.05.003.
27. Guizouarn H, Allegrini B. 2020. Erythroid glucose transport in health and disease. Pflugers Arch 472:1371–1383. https://doi.org/10.1007/s00424-020-02406-0.
28. Lee CF, Caudal A, Abell L, Gowda GAN, Tian R. 2019. Targeting NAD^+ metabolism as interventions for mitochondrial disease. Sci Rep 9:3073. https://doi.org/10.1038/s41598-019-39419-4.
29. Vigueira PA, McCommis KS, Schweitzer GG, Remedi MS, Chambers KT, Fu X, McDonald WG, Cole SL, Colca JR, Kletzien RF, Burgess SC, Finck BN. 2014. Mitochondrial pyruvate carrier 2 hypomorphism in mice leads to defects in glucose-stimulated insulin secretion. Cell Rep 7:2042–2053. https://doi.org/10.1016/j.celrep.2014.05.017.
30. Jiang H, Alahmad A, Fu S, Fu X, Liu Z, Han X, Li L, Song T, Xu M, Liu S, Wang J, Albash B, Alaqeel A, Catalina V, Prokisch H, Taylor RW, McFarland R, Fang F. 2022. Identification and characterization of novel MPC1 gene variants causing mitochondrial pyruvate carrier deficiency. J Inherit Metab Dis 45:264–277. https://doi.org/10.1002/jimd.12462.
31. Song J, Pfanner N, Becker T. 2018. Assembling the mitochondrial ATP synthase. Proc Natl Acad Sci U S A 115:2850–2852. https://doi.org/10.1073/pnas.1801697115.
32. Crane FL. 2001. Biochemical functions of coenzyme Q10. J Am Coll Nutr 20:591–598. https://doi.org/10.1080/07315724.2001.10719063.
33. Xiao D, Zeng L, Yao K, Kong X, Wu G, Yin Y. 2016. The glutamine-alpha-ketoglutarate (AKG) metabolism and its nutritional implications. Amino Acids 48:2067–2080. https://doi.org/10.1007/s00726-016-2254-8.
34. Burch JS, Marcero JR, Maschek JA, Cox JE, Jackson LK, Medlock AE, Phillips JD, Dailey HA, Jr. 2018. Glutamine via α-ketoglutarate dehydrogenase provides succinyl-CoA for heme synthesis during erythropoiesis. Blood 132:987–998. https://doi.org/10.1182/blood-2018-01-829036.
35. Cho J, Seo J, Lim CH, Yang L, Shiratsuchi T, Lee MH, Chowdhury RR, Kasahara H, Kim JS, Oh SP, Lee YJ, Terada N. 2015. Mitochondrial ATP transporter Ant2 depletion impairs erythropoiesis and B lymphopoiesis. Cell Death Differ 22:1437–1450. https://doi.org/10.1038/cdd.2014.230.
36. Karvela M, Baquero P, Kuntz EM, Mukhopadhyay A, Mitchell R, Allan EK, Chan E, Kranc KR, Calabretta B, Salomoni P, Gottlieb E, Holyoake TL, Helgason GV. 2016. ATG7 regulates energy metabolism, differentiation and survival of Philadelphia-chromosome-positive cells. Autophagy 12:936–948. https://doi.org/10.1080/15548627.2016.1162359.
37. Shah DI, Takahashi-Makise N, Cooney JD, Li L, Schultz IJ, Pierce EL, Narla A, Seguin A, Hattangadi SM, Medlock AE, Langer NB, Dailey TA, Hurst SN, Faccenda D, Wiwczar JM, Heggers SK, Vogin G, Chen W, Chen C, Campagna DR, Brugnara C, Zhou Y, Ebert BL, Danial NN, Fleming MD, Ward DM, Campanella M, Dailey HA, Kaplan J, Paw BH. 2012. Mitochondrial Atpif1 regulates haem synthesis in developing erythroblasts. Nature 491:608–612. https://doi.org/10.1038/nature11536.
38. Richard A, Vallin E, Romestaing C, Roussel D, Gandrillon O, Gonin-Giraud S. 2019. Erythroid differentiation displays a peak of energy consumption concomitant with glycolytic metabolism rearrangements. PLoS One 14:e0221472. https://doi.org/10.1371/journal.pone.0221472.
39. Paul BT, Tesfay L, Winkler CR, Torti FM, Torti SV. 2019. Sideroflexin 4 affects Fe-S cluster biogenesis, iron metabolism, mitochondrial respiration and heme biosynthetic enzymes. Sci Rep 9:19634. https://doi.org/10.1038/s41598-019-55907-z.
40. Bader-Meunier B, Miélot F, Breton-Gorius J, Cramer E, Guichard J, Landrieu P, Dommergues JP, Tchernia G. 1999. Hematologic involvement in mitochondrial cytopathies in childhood: a retrospective study of bone marrow smears. Pediatr Res 46:158–162. https://doi.org/10.1203/00006450-199908000-00005.
41. Bench AJ, Nacheva EP, Hood TL, Holden JL, French L, Swanton S, Champion KM, Li J, Whittaker P, Stavrides G, Hunt AR, Huntly BJ, Campbell LJ, Bentley DR, Deloukas P, Green AR. 2000. Chromosome 20 deletions in myeloid malignancies: reduction of the common deleted region, generation of a PAC/BAC contig and identification of candidate genes. UK Cancer Cytogenetics Group Oncogene 19:3902–3913.
42. Braun T, de Botton S, Taksin AL, Park S, Beyne-Rauzy O, Coiteux V, Sapena R, Lazareth A, Leroux G, Guenda K, Cassinat B, Fontenay M, Vey N, Guerci A, Dreyfus F, Bordessoule D, Stamatoullas A, Castaigne S, Terré C, Eclache V, Fenaux P, Adès L. 2011. Characteristics and outcome of myelodysplastic syndromes (MDS) with isolated 20q deletion: a report on 62 cases. Leuk Res 35:863–867. https://doi.org/10.1016/j.leukres.2011.02.008.

43. Fujiwara T, Saitoh H, Inoue A, Kobayashi M, Okitsu Y, Katsuoka Y, Fukuhara N, Onishi Y, Ishizawa K, Ichinohasama R, Harigae H. 2014. 3-Deazaneplanocin A (DZNep), an inhibitor of *S*-adenosylmethionine-dependent methyltransferase, promotes erythroid differentiation. J Biol Chem 289:8121–8134. https://doi.org/10.1074/jbc.M114.548651.
44. Li J, Shima H, Nishizawa H, Ikeda M, Brydun A, Matsumoto M, Kato H, Saiki Y, Liu L, Watanabe-Matsui M, Iemura K, Tanaka K, Shiraki T, Igarashi K. 2018. Phosphorylation of BACH1 switches its function from transcription factor to mitotic chromosome regulator and promotes its interaction with HMMR. Biochem J 475:981–1002. https://doi.org/10.1042/BCJ20170520.
45. Fujiwara T, Okamoto K, Niikuni R, Takahashi K, Okitsu Y, Fukuhara N, Onishi Y, Ishizawa K, Ichinohasama R, Nakamura Y, Nakajima M, Tanaka T, Harigae H. 2014. Effect of 5-aminolevulinic acid on erythropoiesis: a preclinical *in vitro* characterization for the treatment of congenital sideroblastic anemia. Biochem Biophys Res Commun 454:102–108. https://doi.org/10.1016/j.bbrc.2014.10.050.